Wear 301 (2013) 280–289

Contents lists available at SciVerse ScienceDirect

Wear

journal homepage: www.elsevier.com/locate/wear

S-phase against S-phase tribopairs for biomedical applications

J. Buhagiar [a,*], A. Jung [b], D. Gouriou [a], B. Mallia [a], H. Dong [b]

[a] Department of Metallurgy and Materials Engineering, University of Malta, Msida MSD 2080, Malta
[b] School of Metallurgy and Materials, The University of Birmingham, Birmingham B15 2TT, UK

ARTICLE INFO

Article history:
Received 23 August 2012
Received in revised form
30 November 2012
Accepted 8 December 2012
Available online 20 December 2012

Keywords:
S-phase
Expanded austenite
Corrosion–wear
Austenitic stainless steel
Carburising
Nitriding

ABSTRACT

S-phase, or expanded austenite, is a corrosion resistant diffused hardened layer which can be created in austenitic stainless steels and cobalt–chromium(Co-Cr) alloys. It is a precipitate-free metastable supersaturated solid solution of nitrogen or carbon or both. S-phase layers formed on biomedical grade austenitic stainless steels have demonstrated significantly enhanced in-vitro wear and corrosion properties. To date, all these tribo-corrosion studies on S-phase treated alloys were conducted using an alumina or tungsten carbide ball as the counterface material. Testing S-phase against S-phase is both scientifically interesting and technologically important in view of their potential applications for the articulating surfaces of metal-on-metal joint prostheses. In this work, biomedical grade 316LVM and High-N stainless steel discs together with AISI 316 balls were low temperature plasma surface alloyed with: nitrogen (nitriding); carbon (carburising); and both carbon and nitrogen (carbonitriding). The S-phase layers created by these treatments were in-vitro corrosion–wear tested in Ringer's solution using an S-phase engineered ball reciprocating against an S-phase engineered disc. In addition, self-mated tribopairs of untreated stainless steel and Co–Cr alloy were used as benchmarks. The results demonstrate that the self-mated S-phase tribopairs can produce a marked decrease in material loss when compared to self-mated untreated stainless steel tribopairs. This is partially because of significantly increased surface hardness and thus an enhanced mechanical support for the surface oxide film. The combined wear loss of the S-phase stainless steel tribopairs was close to that of the benchmark Co–Cr tribopair. It can be concluded from this work that S-phase surface engineering can effectively combat scuffing or seizure of biomedical austenitic stainless steels when self mated. Therefore S-phase hardened austenitic stainless steels could compete against more expensive alloys such as Co–Cr alloys in metal-on-metal wear applications in the biomedical industry.

1. Introduction

Austenitic stainless steels display excellent corrosion resistance and are frequently used in corrosion–wear environments. They find applications in the chemical, petrochemical, medical and food processing industries. For instance, austenitic stainless steels can be found as a main material in pumps, valves, bearings, fasteners and conveyor belts, where one contacting metal surface moves relative to the other [1]. However, austenitic stainless steels are characterized as having relatively poor wear resistance in sliding contact.

The low hardness and poor tribological properties of austenitic stainless steels were overcome in 1985, when Zhang and Bell [2] developed a low temperature plasma nitriding process to form a so called S-phase (or expanded austenite) surface layer, which increases the hardness and wear resistance of austenitic stainless steels without any detriment to their corrosion resistance. Later work by Lewis et al. [3] showed that S-phase can also be formed by low temperature carburising and in 2000 Blawert et al. [4] reported that plasma alloying with both nitrogen and carbon created a hybrid S-phase layer which inherited the advantages of both nitriding and carburising.

Thaiwatthana et al. [5] reported that both nitrogen and carbon rich S-phase can significantly improve the corrosion–wear resistance of austenitic stainless steel. Corrosion–wear experiments at Leeds University on S-phase coatings by Aldrich-Smith and Dearnley [6] have demonstrated that when using a WC–Co ball as counterface in 3 wt% NaCl the S-phase coatings slightly improved the corrosion–wear resistance of the uncoated 316L stainless steel. However when rubbing against an alumina ball, S-phase coatings improved the corrosion–wear resistance of the untreated 316L stainless steel vastly. Clearly, the counterface has played an important role in determining the corrosion–wear behaviour of S-phase layers.

Lately metal-on-metal hip implants, which were deemed as more effective in reducing the wear debris than metal-on-polymer joints, were at the epicentre of a controversy due to their high

* Corresponding author. Tel.: +356 2340 2439; fax: +356 2134 3577.
E-mail address: joseph.p.buhagiar@um.edu.mt (J. Buhagiar).

0043-1648/$ - see front matter © 2012 Elsevier B.V. All rights reserved.
http://dx.doi.org/10.1016/j.wear.2012.12.012

failure rates [7]. However a reply to the paper by Smith et al. [7] has initiated a debate whether the high failure rate was material or design related [8,9].

It should also be indicated that in real hip-joint applications it is very rare for stainless steel surfaces to be sliding against alumina ceramics or WC–Co composites. In addition, it has also been reported that S-phase tribopairs can be used to reduce food contamination by the rubber ring seal used in stainless steel dosing pumps [10]. This application could be extrapolated to the biomedical implant industry if further studies on the metal-on-metal implant controversy [7–9,11] reveal that the problem was only design related. In fact there is no real agreement on the reason of the high failure rates of metal-on-metal implants. An increase in the surface hardness without any deterioration of the corrosion resistance could solve the problem.

To this end, corrosion–wear studies of a tribopair both made of S-phase layers were conducted in this work for the first time. Co–Cr ball against Co–Cr disc were used as the benchmark because Co–Cr based alloys have been successful used in metal-on-metal joint prostheses and in the chemical, petrochemical, medical and food processing industries [12].

2. Material and methods

2.1. Materials and surface treatments

The main materials (chemical composition in Table 1) used in this work were biomedical grade ASTM F138 (Sandvik Bioline 316LVM) and ASTM F1586 (Sandvik Bioline High-N) annealed stainless steel bars (ø25 mm) and AISI 316 stainless steel balls (ø12.7 mm, Spheric Trafalgar). In order to compare the results against a tribopair which is well renowned for its excellent metal-on-metal corrosion–wear properties, a cast Co–Cr ASTM75 alloy disc was made to reciprocate against a HIPped powder metallurgy Co–Cr Stellite®6 ball.

Disc samples of 6 mm in thickness were cut from the annealed stainless steel bars (ø25 mm) and one flat surface of the discs was wet ground using silicon carbide papers from 120 down to 1200 grit. The samples (discs and balls) were ultrasonically cleaned in acetone and dried with hot air prior to low temperature plasma surface alloying (LTPSA) to form the S-phase layers. The samples were placed in a specially designed jig, shown in Fig. 1, and were subjected to three different LTPSA treatments: (i) with nitrogen (N430); (ii) with carbon (C500) and (iii) with both nitrogen and carbon (NC430). The process conditions (Table 2) were chosen based on our previous work, on the fact that a biocompatible precipitate free S-phase can be formed on austenitic stainless steel by LTPSA under the same conditions [13–15].

Following the surface treatments, all treated and untreated samples were gently polished to remove a back-deposited superficial layer as explained in Ref. [14]. Transmission electron microscope (TEM) observation in our previous work [14] revealed that this back deposited layer consisted of extremely fine equiaxed grains with a diameter of 5–10 nm and with a thickness of 50 nm. Its structure can be assigned to an fcc structured M(N,C) where M=Fe, Cr, Ni, Mo and Mn. Polishing was conducted on a Streurs LaboPol-5 automatic polisher using 6 μm diamond paste with a medium force (mark 3) for 5 min. This was followed by a final polishing at a low force (mark 1) using 1 μm diamond paste for another 3 min. In order to gauge the thickness of material removed, a 1 μm GDOES hole was sputtered, measured with a profilometer and then the sample was polished until the mark was no longer visible. Using this polishing technique for all the

Table 2
LTPSA process parameters.

Code	Process Parameters						
	Furnace (kW)	Temperature (°C)	Time (h)	Pressure (Pa)	Gas Mix (%)		
					CH_4	N_2	H_2
N430	60	430	15	400	0	25	75
NC430	60	430	15	400	1.5	25	73.5
C500	40	500	15	400	1.5	0	98.5

Table 1
Material composition.

Material	Composition (wt%)										
	Type	C	Si	Mn	P	S	Cr	Ni	Mo	N	W	Bal
ASTM F138	bar	0.019	0.5	1.87	0.018	0.001	17.43	13.75	2.72	0.084	–	Fe
ASTM F1586	bar	0.037	0.47	3.99	0.018	0.0013	20.80	9.82	2.33	0.39	–	Fe
AISI 316	ball	0.08 max	1.0 max	2.0 max	0.045 max	0.03 max	16–18	10–14	2–3	–	–	Fe
ASTM F75	bar	0.35 max	1.0 max	1.0 max	0.02 max	0.01 max	26.5–30	0.5 max	4.5–7	0.25 max	1.0	Co
Stellite® 6	ball	1.24	0.77	–	–	–	29.3	2.6	–	–	4.5	Co

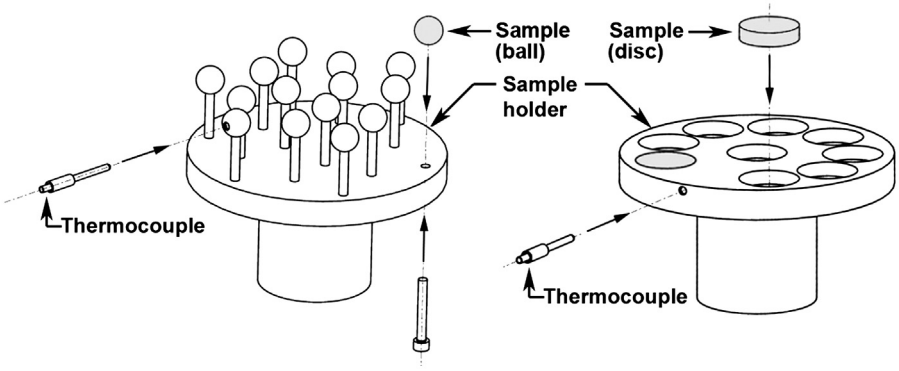

Fig. 1. Jigs for sample (ball and disc) treatment.

samples, made sure that less than 1 μm of the layer was removed and the surface finish (Ra) of all the polished samples was between 0.06 and 0.10 μm.

2.2. Materials characterisation

Standard procedures were followed to prepare metallographic specimens to be examined under a Leitz DMRX optical microscope. This included cross-sectioning normal to the surface, mounting in phenolic resin, wet grinding with silicon carbide paper, polishing and etching in a solution containing 50 ml of HCl (39% conc.), 25 ml of HNO_3 (69% conc.) and 25 ml of distilled water.

Surface hardness was measured using a Mitutoyo MVK-H1 micro-hardness tester with a Vickers indenter at a range of loads varying between 0.025 and 1 kgf with three repeats for each measurement. A computer controlled Nano-Test 600 machine (Micromaterials, UK) was used to evaluate the surface hardness of the as-received and plasma surface alloyed samples. The indentation tests were carried out normal to the surface and 15 points were selected in order to determine the hardness values.

2.3. Reciprocating wear test

Polished (Ra=0.06–0.1 μm) treated and untreated disc coupons were cut into blocks of 5 mm by 7 mm by 6 mm. The samples were then glued (Struers–Tripod wax) to another block and the treated surface was masked by tape. The assembly was then clamped into the holder and was spray lacquered. When the lacquer dried the masking tape was removed and the sample surface was cleaned with acetone.

In this test, treated and untreated AISI 316 balls were used. Also a Co–Cr tribopair was used as a benchmark. Before testing the treated balls were slightly polished with 0.25 μm diamond paste and then washed in acetone, whilst the untreated balls were used as supplied. During the reciprocating wear test, the disc sample was made to move linearly against a stationary treated or untreated stainless steel ball of 12.7 mm in diameter at an average speed of 12.5 mms^{-1} (1 Hz) for 200 m at 25 °C in Ringer's solution (0.1540 M NaCl; 0.0056 M KCl; 0.0043 M $CaCl_2$; 0.0024 M $NaHCO_3$). In order to prepare 1 L Ringer's solution, eight, one quarter strength LAB100Z Ringer's solution tablets supplied by Lab M (UK) were used. The normal contact load acting on the ball was of 39 N and a wear scar of 6 mm in length (oscillation amplitude) was produced. The test was repeated two times per condition.

The initial Hertzian contact pressures for the reciprocating-wear tests were calculated. The values obtained for the stainless tribopair and Co–Cr tribopair were of 1.40 GPa and 1.44 GPa, respectively. This high Hertzian stress is not representative of the joint replacement environment. However this load was necessary in order to be able to have a measurable wear on the treated specimens within a reasonable testing period of 4 h 26 min. Post-wear examination of the cross-sections of the wear tracks was conducted on all specimens and no gross plastic deformation could be detected within the microstructure close to the tested surface.

The cross-sectional area of the wear area was determined by measuring the cross-section of a wear track using a stylus profilometer. To obtain the wear volume, the area of the wear scar was calculated using Simpson's rule and then was multiplied by the length of the wear track. Three measurements were performed for each wear track and the average value is reported. The wear volume lost from the ball was calculated using a geometrical method that takes in consideration the projected diameter of the wear scar and the diameter of the ball. The morphologies of the wear scars were characterized by a Zeiss Merlin field emission Scanning electron microscope (SEM) with an EDX capability.

3. Results

3.1. Microstructure

The cross-section microstructures shown in Figs. 2 and 3 reveal the surface layers formed on ASTM F138 and ASTM F1586, respectively. The surface modified layer in most treated samples appears to be bright white. This is an indication that the surface layer has superior corrosion properties to the untreated material when etched [10]. The distinct line at the substrate–layer interface, especially in the nitrided (Figs. 2a and 3a) and carbonitrided (Figs. 2b and 3b) layers and to a lesser extent in the carburised (Figs. 2c and 3c) layers, is due to grinding and

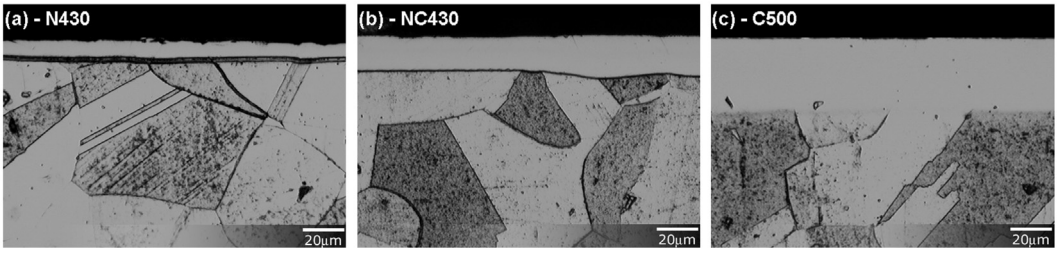

Fig. 2. Microstructure of S-phase layers formed by (a) nitriding, (b) carbonitriding and (c) carburising on ASTM F138 discs.

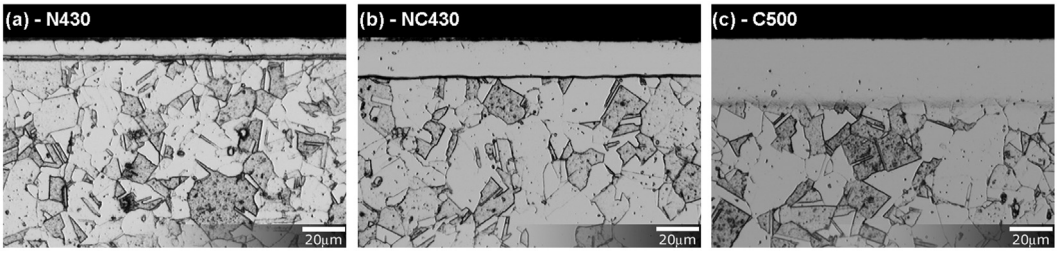

Fig. 3. Microstructure of S-phase layers formed by (a) nitriding, (b) carbonitriding and (c) carburising on ASTM F1586 discs.

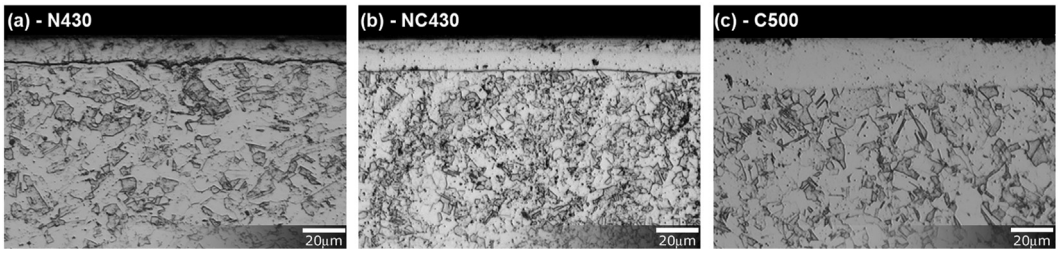

Fig. 4. Microstructure of S-phase layers formed by (a) nitriding, (b) carbonitriding and (c) carburising on AISI 316 balls.

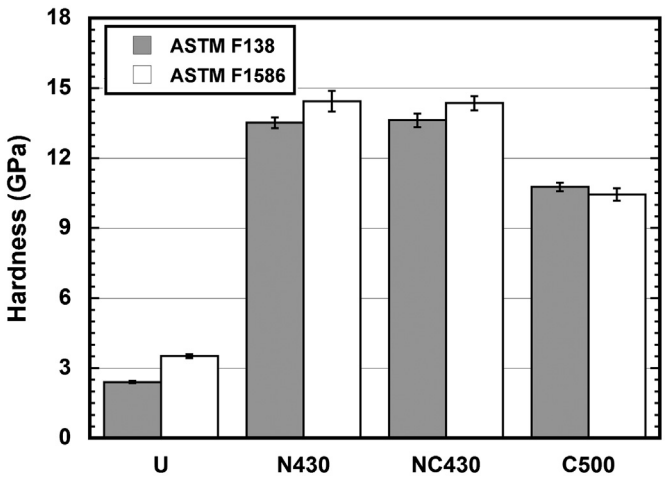

Fig. 5. Nano-hardness of treated and untreated ASTM F138 and F1586 discs. Error bar: standard deviation of 15 values.

polishing where a step was formed because of the difference in hardness between the hard S-phase layer and the soft substrate.

For the nitrided balls at 430 °C the S-phase layer formed (Fig. 4a) is not completely white and this implies that there are some precipitates within it. Fig. 4b shows the cross-section of a carbonitrided ball and the S-phase layer is white in the bottom region and not completely white in the top-part. It is known that the whole S-phase case produced by hybrid carbonitriding consists of a top N-rich S-phase layer followed by a C-rich S-phase sublayer [10,14]. This implies that this S-phase case has precipitates in the nitrogen-rich part of the S-phase layer and is precipitate free in the carbon-rich part of the S-phase sublayer. The carburised layer shown in Fig. 4c on the other hand seems to be precipitate free.

Due to the hemispherical nature of the surface of the ball it was impossible to conduct any further characterisation using XRD and GDOES. The only evidence that S-phase had formed in these balls lies in the microscopic examination and hardness measurements.

3.2. Surface mechanical properties

Fig. 5 summarizes the nano-indentation results for ASTM F138 and F1586 discs treated using three different processes. It can be clearly seen that these alloys can be hardened significantly using any of these surface alloying processes. It can be seen that the carburised surfaces (C500) are not so hard as nitrided (N430) and carbonitrided (NC430) surfaces and that both ASTM F138 and ASTM F1586 exhibited very similar hardening response to all these three plasma surface alloying processes. Fig. 6 shows the load bearing capacity of treated and untreated ASTM F138 and ASTM F1586. The effective surface hardness of the nitrided specimens decreased quickly when the indentation load was

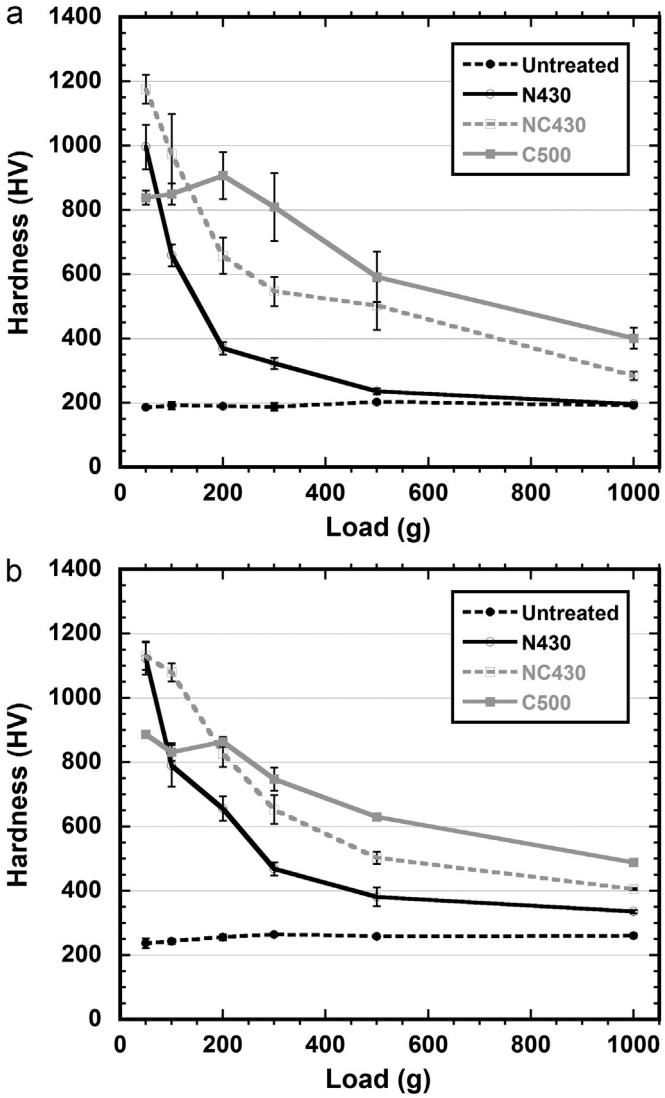

Fig. 6. Surface micro-hardness at different loads of treated and untreated ASTM F138 (a) and F1586 discs (b). Error bar: deviation from mean of three values.

above 100 g, indication of its relatively low load bearing capacity. On the other hand, the 500 °C carburised layer showed a lower effective surface hardness relative to the nitrided layer under a low load (<200 g) but the highest load bearing capacity at higher loads. This phenomenon occurs because the carburised layer was thicker than the nitrided layer (Figs. 2 and 3).

Due to the relatively high roughness of the surface of the ball it was impossible to conduct nano-indentation. Utilising a load of 100 g the hardness of the treated AISI 316 balls were measured to be: 990 ± 80 $HV_{0.1}$ for N430; 905 ± 85 $HV_{0.1}$ for NC430; and 713 ± 19 $HV_{0.1}$ for C500. The untreated AISI 316 and CoCr balls

had a hardness of 200 ± 10 $HV_{0.1}$ and 424 ± 9 $HV_{0.1}$ respectively. The CoCr disc material had a hardness of 305 ± 13 $HV_{0.1}$.

3.3. Corrosion–wear

3.3.1. Wear loss of discs

The wear loss of surface treated and untreated disc samples can be compared from Fig. 7. The wear loss of the untreated ASTM F138 disc against the untreated AISI 316 ball is very high whilst the wear loss of the untreated ASTM F1586 disc is only about 25% that of untreated ASTM F138 disc when tested under the same conditions. On the other hand, it was observed that all treated disc samples showed excellent wear resistance when sliding against treated balls.

For the ASTM F138 discs the treatments decreased their wear drastically but was still inferior to the Co–Cr tribopair. When compared to ASTM F138, the wear resistance improvement of the treated ASTM F1586 discs over the untreated material was not so large; however the wear properties were more sensitive to the treatment conditions. With the exception of the C500|N430 tribopair all the treated ASTM F1586 discs showed superior or comparable wear resistance when compared to the Co–Cr benchmark.

3.3.2. Wear loss of balls

The wear loss of the AISI 316 balls sliding against discs made from two different materials and treated by three different conditions is summarised in Fig. 8. It can be clearly seen that the wear loss of the untreated balls rubbing against the untreated discs (i.e. U|U) was much larger when compared to any S-phase tribopair. In fact all three plasma surface treatments, C500, N430 and NC430, can effectively improve the wear resistance of AISI 316 balls sliding in Ringer's solution against the treated austenitic stainless steel discs.

The wear loss of the untreated AISI 316 ball sliding against an untreated ASTM F138 disc was higher when compared to sliding against an untreated ASTM F1586 disc. This is in agreement with the wear loss results of discs shown in Fig. 7. However for the treated AISI 316 balls sliding against treated discs the opposite happened. Sliding against a treated ASTM F138 discs always resulted in a higher wear loss when compared to sliding against a treated ASTM F1586 disc.

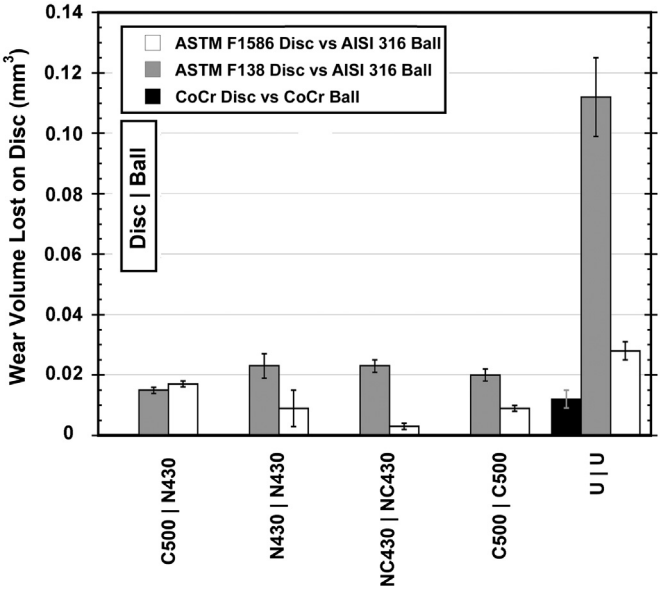

Fig. 7. Wear volume loss of disc after reciprocating wear tests in Ringer's solution. Error bar: deviation from mean of two values.

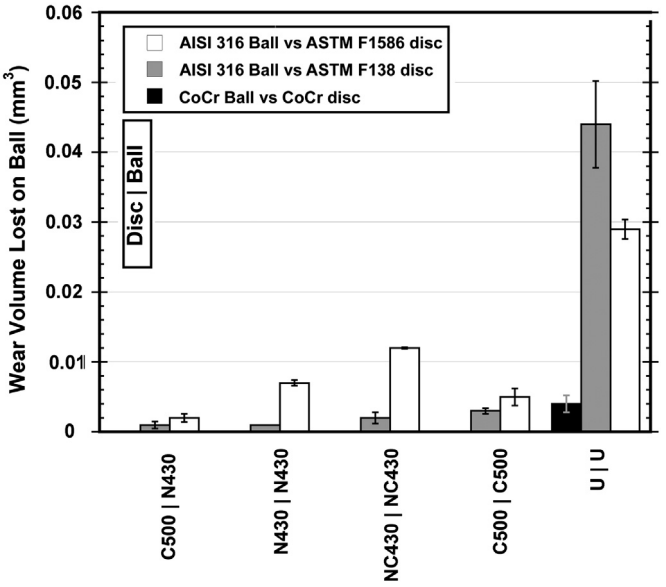

Fig. 8. Wear volume loss of ball after reciprocating wear tests in Ringer's solution. Error bar: deviation from mean of two values.

In fact all the treated AISI 316 balls sliding against treated ASTM F138 discs showed wear volumes comparable to and sometimes lower than the Co–Cr benchmark. The same could not be told for some of the treated balls sliding against treated ASTM F1586 discs.

3.3.3. Combined wear

The combined wear volume loss of the balls and discs together is illustrated in the stacked bar chart in Fig. 9. It was observed that for nearly all the samples tested, whether they were surface treated or not, the wear of the AISI 316 balls is much less than that of the counterface discs. The combined wear of three plasma treated tribopairs made of ASTM F1586 (N430|N430, NC430|NC430 and C500|C500) and one plasma treated tribopair (C500|N430) made of ASTM F138 is close to that of Co–Cr tribopair, which is the material of choice for metal-on-metal joint prostheses. However the tribopairs that are inferior to the Co–Cr tribopair are still very close and therefore the selection of the best tribopair can only be made by observing the wear morphologies.

3.4. Wear morphologies

3.4.1. Co–Cr tribopair

The wear morphology of the Co–Cr tribopair samples after the tribo-corrosion test can be seen in Fig. 10. The wear on the disc (Fig. 10a) is of an abrasive nature characterised by mild abrasion marks in the direction of sliding. Some oxidation can be seen on the surface (dark streaks, 2 wt% of oxygen) and at higher magnifications mud-like cracking of the oxide can be observed (not shown). The ball (Fig. 10b) contained grooves in the direction of sliding together with some cracking around secondary phases ($Cr_{23}C_6$) in the microstructure. This wear mechanism dominated by mild abrasion on both disc and ball is in line with the very low wear of the tribopair (Fig. 9).

3.4.2. Untreated stainless steel tribopair

Fig. 11 shows the corrosion–wear morphology of the untreated ASTM F138–AISI 316 tribopair (U|U). The wear track of both disc (Fig. 11a) and ball (Fig. 11b) are characterised by abrasion marks in the direction of sliding, material tearing and local failure due to

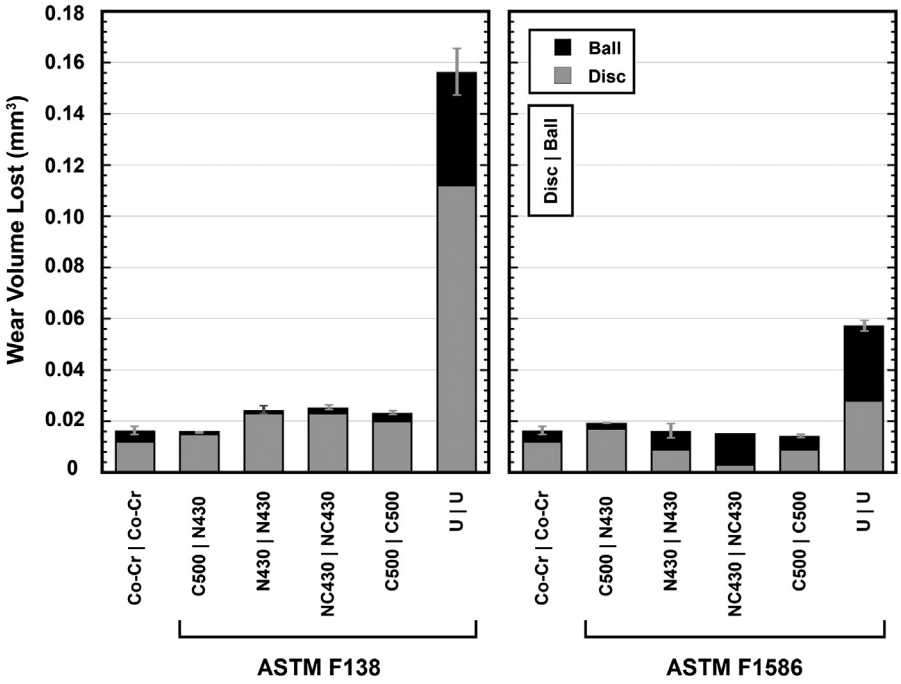

Fig. 9. Combined wear volume loss of disc and ball. Error bar: deviation from mean of two values of the combined wear lost.

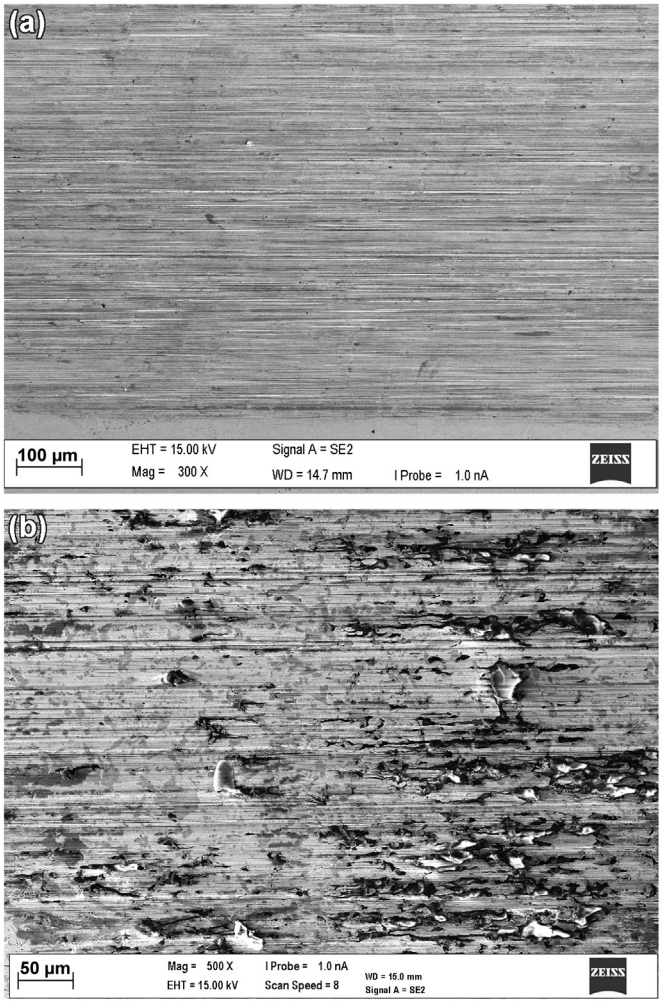

Fig. 10. SEM images of wear morphology on (a) disk (b) ball of the Co–Cr tribopair. Direction of sliding: left to right.

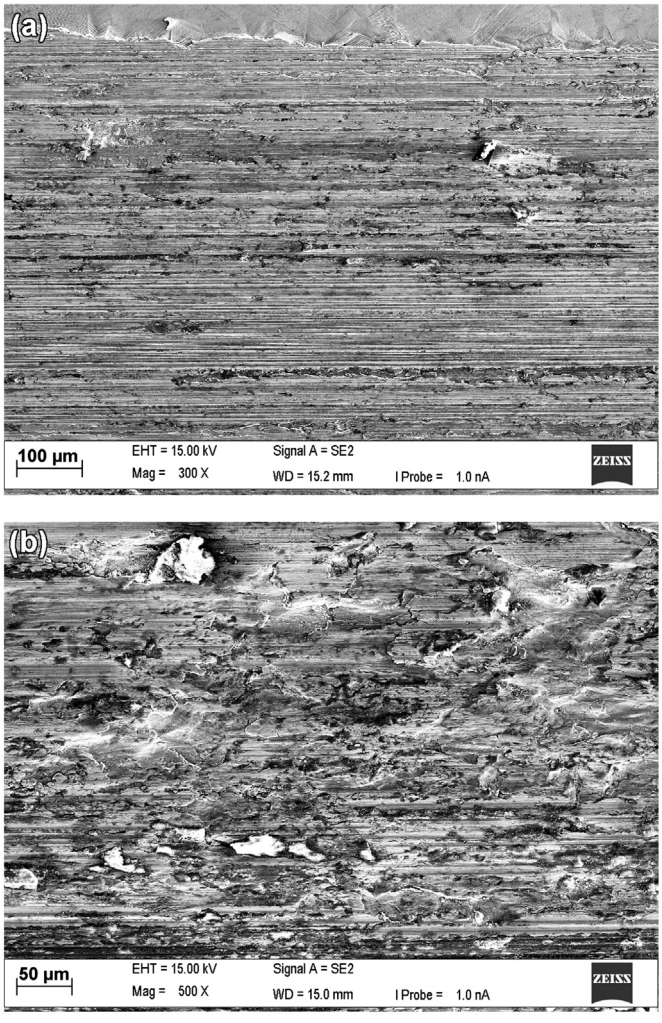

Fig. 11. SEM images of wear morphology on (a) untreated ASTM F138 disc and (b) untreated AISI 316 ball tribopair (U|U). Direction of sliding: left to right.

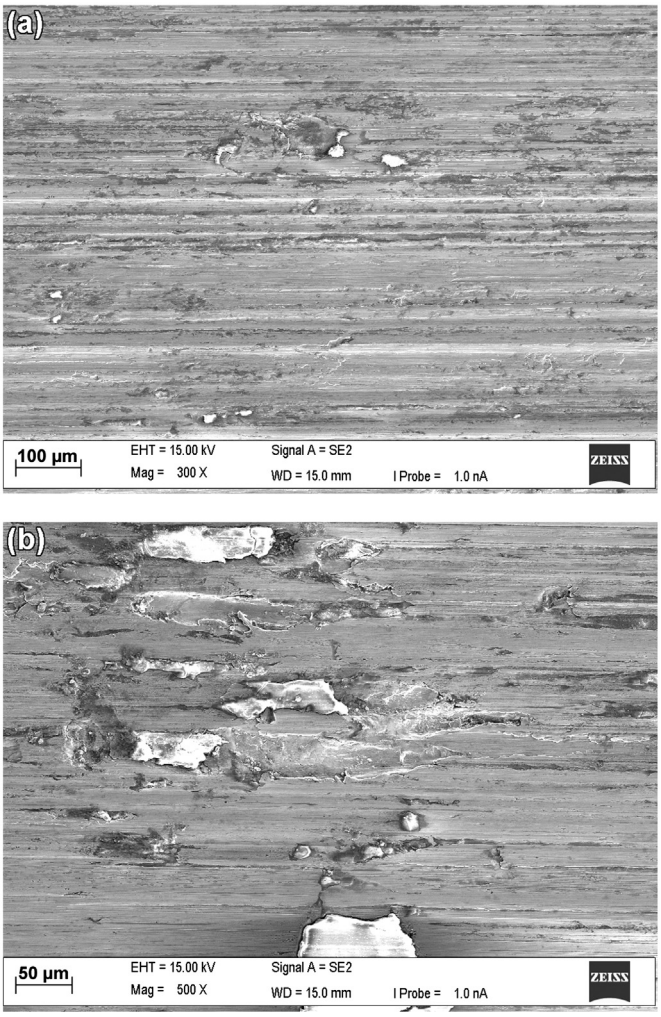

Fig. 12. SEM images of wear morphology on (a) untreated ASTM F1586 disc and (b) untreated AISI 316 ball tribopair (U|U). Direction of sliding: left to right.

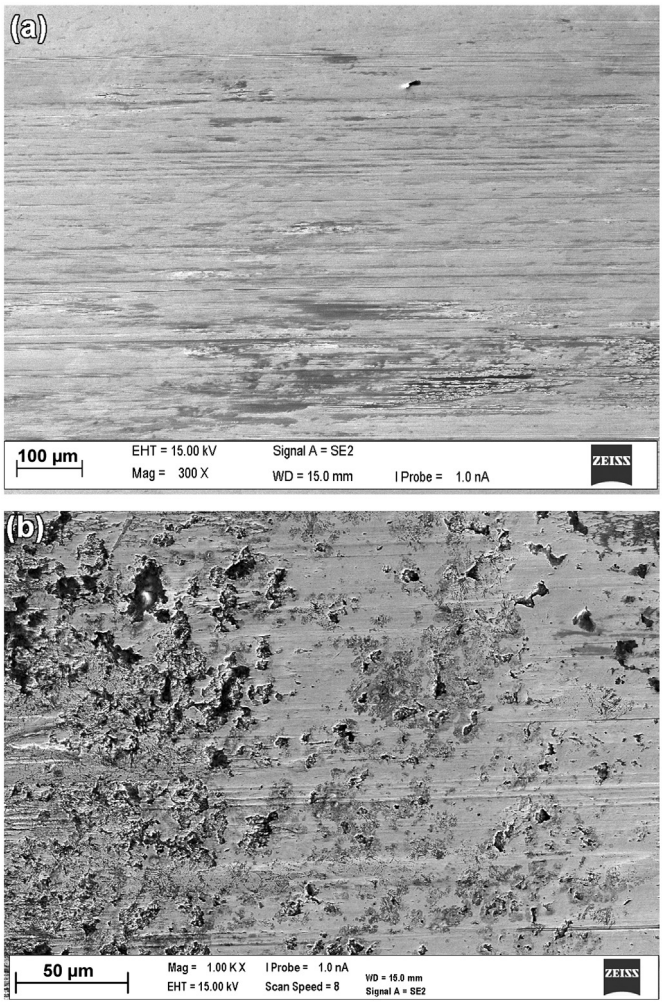

Fig. 13. SEM images of wear morphology on (a) ASTM F138 carburised disk and (b) AISI 316 carburised ball tribopair (C500|C500). Direction of sliding: left to right.

Table 3
Observed wear mechanisms via SEM.

Disc|Ball	ASTM F138–AISI 316 Tribopair		ASTM F1586–AISI 316 Tribopair	
	Disc	Ball	Disc	Ball
U|U	Delamination Abrasion (severe) Adhesion (severe) Oxidation	Delamination Abrasion (severe) Roughening (severe) Oxidation	Delamination Abrasion (severe) Adhesion (minor) Oxidation	Delamination Abrasion (severe) Roughening (mild) Oxidation
C500|C500	Abrasion (mild) Oxidation	Abrasion (mild) Oxidation	Abrasion (mild) Oxidation	Abrasion (mild) Oxidation
C500|N430	Abrasion (polishing) Oxidation	Abrasion (mild) Cracking of layer Oxidation	Abrasion (polishing) Oxidation	Abrasion (mild) Cracking of layer Oxidation
N430|N430	Delaminaton Cracking of layer Oxidation	Abrasion (polishing) Cracking of layer Oxidation	Abrasion (polishing) Cracking of layer Etching and Oxidation	Abrasion (polishing) Cracking of layer Oxidation
NC430|NC430	Abrasion (mild) Etching Oxidation	Abrasion (mild) Cracking of layer Oxidation	Abrasion (polishing) Etching Oxidation	Abrasion (mild) Oxidation

repeated plastic deformation. Delamination, due to the work hardening of the surface resulting in subsurface cracks which then propagate towards the surface, was observed. Adhesive transfer at the start and end of the wear scar was also observed (not shown). Flat debris generated via delamination due to the repeated rubbing action was transferred to the ball resulting in roughening of the ball (Fig. 11b) and aggravated abrasion of the disc. Fine (1 μm) wear debris deposition layer could be observed outside of the wear track.

The untreated ASTM F1586–AISI 316 tribopair (U|U), Fig. 12, showed very similar wear mechanisms to the ASTM F138–AISI 316 tribopair (U|U), Fig. 11; however the severity of damage was much less. The abrasion marks in the direction of sliding, delamination and adhesive transfer are in fact much less. The ball counterface, Fig. 12b, also had much less roughening when compared to that of Fig. 11b. When compared with the Co–Cr benchmark tribopair the severity of the wear in both the untreated stainless steel tribopairs was much higher. Both observations are in agreement with the results presented in Fig. 9.

3.4.3. *Treated stainless steel tribopairs*

The wear tracks, disc and ball, of all the treated tribopairs were observed via SEM and the principal wear mechanisms were studied. Table 3 summarises these observations; however in this paper only C500|C500 and C500|N430 will be discussed in detail.

Figs. 13 and 14 show the wear morphology on carburised AISI 316 balls against carburised ASTM F138 and ASTM F1586 discs, respectively. It can be clearly seen that the discs (Figs. 13a and 14a) and balls (Figs. 13b and 14b) were suffered from mild abrasion in the direction of sliding which is accompanied by oxidation (dark coloured streaks, ASTM F138 C500: 3.1 wt% oxygen, ASTM F1586 C500: 18.5 wt% oxygen and ball: 5.0 wt% oxygen). No evidence of adhesive failure can be seen in any part of the wear track. The severity of the wear on the disc shown in Fig. 14a is much lower than that shown in Fig. 13a. This is in agreement with the results shown in Fig. 9.

Figs. 13b and 14b show the wear morphology on the ball. Mild abrasive marks in the direction of sliding can be seen together with black spots covering the surface. These black spots are more frequent on the ball that was sliding on the carburised ASTM F138 disc. These black spots (5.0 wt% oxygen) might be oxidised wear debris that were smudged on the surface.

Figs. 15 and 16 show the wear morphology on nitrided AISI 316 balls against carburised ASTM F138 and ASTM F1586 discs, respectively. The discs, undergone mild abrasive (polishing) wear (Figs. 15a and 16a) together with mild oxidation (dark black spots and streaks, ASTM F138 C500: 3.2 wt% oxygen and ASTM F1586 C500: 3.0 wt% oxygen). The balls, on the other hand, suffered from mild abrasion, slight oxidation and cracking of the surface. These cracks are always perpendicular to the direction of sliding. The

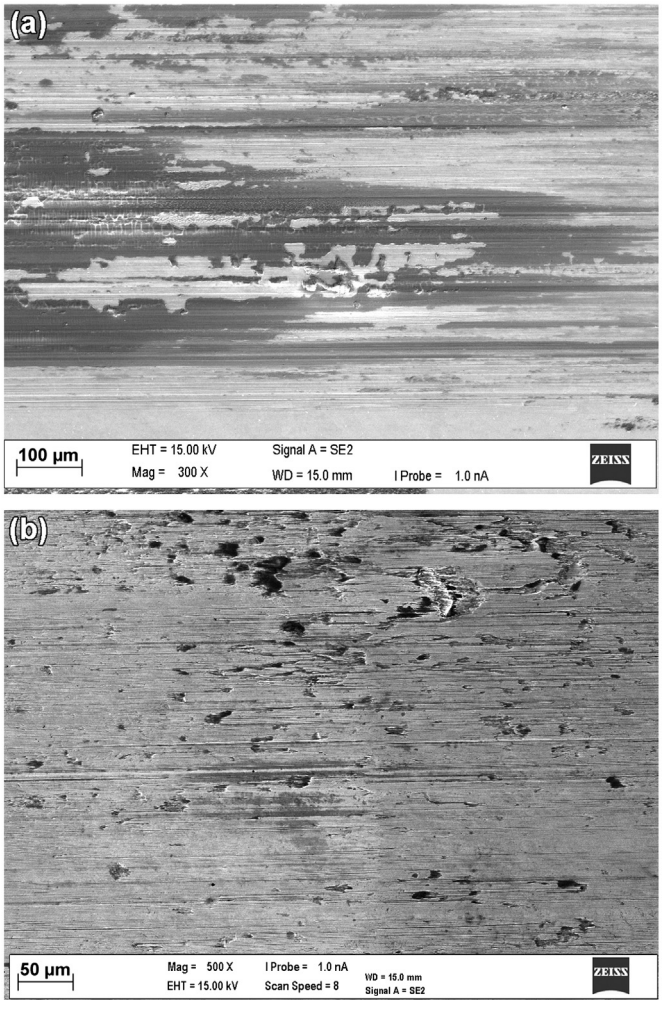

Fig. 14. SEM images of wear morphology on (a) ASTM F1586 carburised disk and (b) AISI 316 carburised ball tribopair (C500|C500). Direction of sliding: left to right.

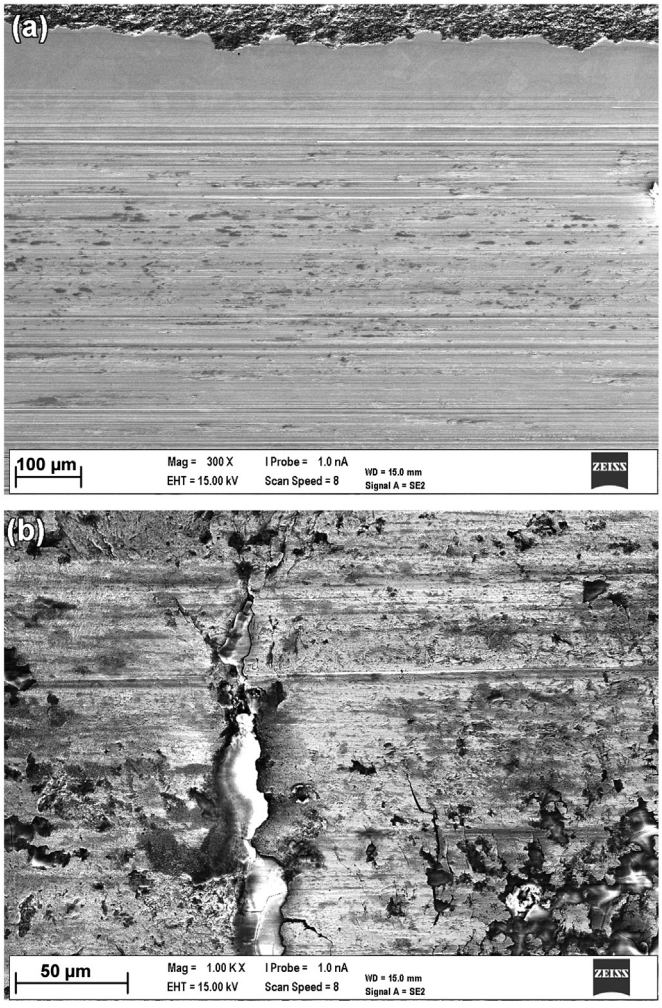

Fig. 15. SEM images of wear morphology on (a) ASTM F138 carburised disk and (b) AISI 316 nitrided ball tribopair (C500|N430).

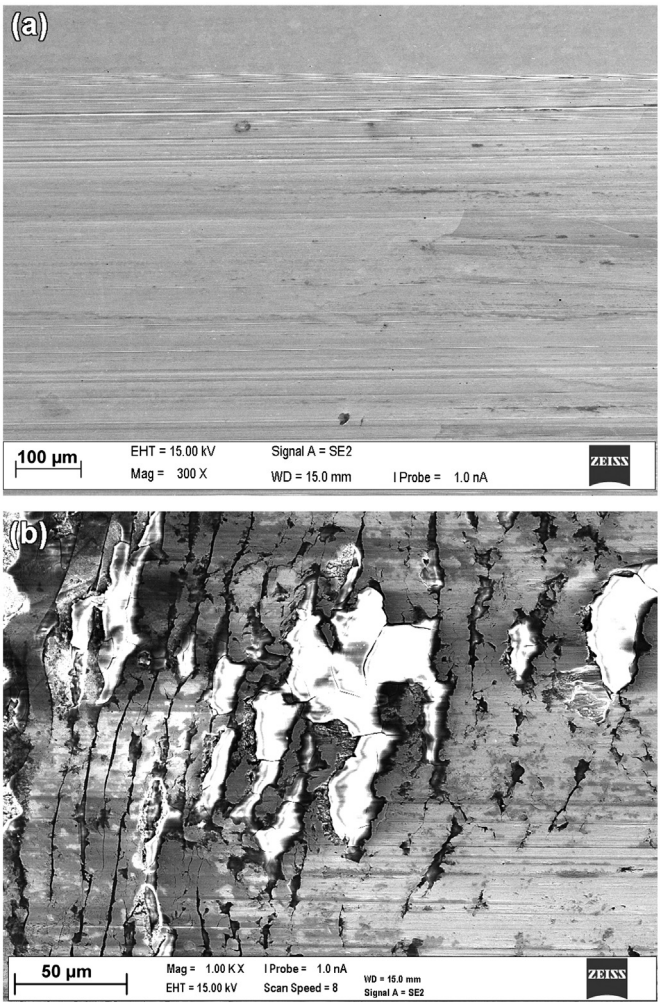

Fig. 16. SEM images of wear morphology on (a) ASTM F1586 carburised disk and (b) AISI 316 nitrided ball tribopair (C500|N430).

surface cracks on the nitrided AISI 316 balls are more pronounced in the tribopair that contained an ASTM F1586 disc (Fig. 16b) than the ASTM F138 one (Fig. 15b).

4. Discussion

4.1. Mechanical properties

The hardness values, shown in Fig. 5, have indicated that the untreated ASTM F1586 is harder than the untreated ASTM F138. This difference in hardness is related to the material composition of the alloys. A higher amount of interstitial nitrogen present in ASTM F1586 (0.39 wt%, Table 1) when compared to ASTM F138 (0.084 wt%, Table 1) increases the proof strength. From the material certificate (Sandvik Bioline) the values of the proof strength (at 0.2%) for untreated ASTM F138 and F1586 are 300 MPa and 587 MPa respectively. This is in line with our hardness measurements.

The load bearing capacity plots, shown in Fig. 6, have demonstrated that the carburised layers can support a higher load than the nitrided layers. This is due to the fact that the carburised layer formed at 500 °C is much thicker than the nitrided layer and therefore can support the indentation load better (Figs. 2c and 3c). With the strong support by the underlying C-enriched layer (Figs. 2b and 3b), the carbonitrided treated surfaces exhibited a much enhanced load bearing capacity as compared to the 430 °C nitrided surfaces. This is because the carbonitrided layers are thicker than the nitrided layers (Figs. 2 and 3).

4.2. Wear volumes

When the wear volumes of the balls are added to those of the discs the differences between the two materials are less defined. This can be explained by two possible reasons. Firstly because the treated ASTM F138–AISI 316 and treated ASTM F1586–AISI 316 tribopairs behaved in an opposite manner, with high wear loss on disc and a low wear loss on balls for the former and low wear loss on disc and a high wear loss on balls for the latter (Figs. 7 and 8). These two therefore slightly compensate for each other. Secondly the error bars are addition of the scatter of two separate measurements. This makes the error bars larger and this increases the variability in results. Choosing the best tribopair by wear loss becomes a challenge and therefore selection by wear morphology may become more important.

4.3. Wear mechanisms

From the results section it is clear that a treated tribopair, no matter which material or treatment condition is selected, can confer combined wear resistance comparable to the Co–Cr benchmark. The reason for this improved wear resistance is due to a change of wear mechanism which differs from what normally happens in untreated stainless steel but is more similar to that observed in Co–Cr alloys.

In the untreated tribopair, the ASTM F138 material suffered from severe delamination which generated wear debris that were transferred to the ball. This transfer of material resulted in severe roughening of the ball which in turn caused aggravated abrasion of the disc. A similar wear mechanism occurred on the ASTM F1586 but was much less severe; in fact the wear volume was much lower for untreated ASTM F1586 than for ASTM F138 (Fig. 7). Higher proof strength, 587 MPa for ASTM F1586 when compared to the 300 MPa for ASTM F138, is also an indication of higher shear yield strength. Due to this higher shear yield strength, more cycles are required to result in delamination of the surface.

Delamination wear did not occur in any of the treated stainless steel discs and therefore very low wear loss was observed (Fig. 7). This is due to the fact that the treated stainless steel surfaces are hard (Figs. 5 and 6) and therefore the yield strength and the shear yield strength of the material are much improved. The S-phase microstructure is composed of entangled dislocations and a high density of stacking faults and this decreases the tendency of cross slip [14]. Therefore the S-phase treated tribopairs do not have a tendency to work harden further because dislocation cross slip is hindered by the presence of stacking faults and entanglement of dislocations.

For the untreated stainless steel tribopairs, especially at the start and end of the wear tracks, adhesive failure was noticed. This could be partially attributed to the fact that the untreated balls and discs have very similar metallurgical characteristics and thus high metallurgical compatibility. According to Rabinowicz's [16] adhesive wear theory, severe adhesive wear will occur because of the very large metallurgical compatibility between them. Also, due to the fact that austenitic stainless steels are very soft, ductile and prone to work hardening they have a high tendency for adhesive wear. The surface oxide films on the untreated austenitic stainless steels tribopairs will be easily damaged and removed under the mechanical interaction due to the lack of the necessary mechanical support from the substrate. This leads to direct rubbing of metal-against-metal, which in turns creates adhesion of the asperities of

the two rubbing faces. Because austenitic stainless steels are very ductile, growth of adhesive junctions is fast, thus giving rise to material transfer and severe adhesive wear of the untreated surfaces [17].

Work hardening of the transferred material on the counterpart ball will occur during the sliding process due to the low stack fault energy and strong work hardening tendency of austenitic stainless steels. These hardened transferred materials will abrade the soft disc, thus leading to abrasive wear as evidenced in Figs. 11 and 12.

The combined wear of discs and balls can be effectively reduced by plasma surface alloying the surfaces of both disc and ball (Fig. 9). Such improvement in wear performance can be explained from the change of the wear mechanism. In general the treated discs against the treated balls experienced a very mild abrasive wear with some oxidation (Table 3). This change in mechanisms is attributed to the strong mechanical support from hardened S-phase layer (Fig. 6) to the surface passive film, which could avoid direct metal-on-metal contact in stainless steel tribopairs. This is in contrast to the untreated tribopair on which the oxide film would be easily removed by the rubbing of the hard asperities from the ball and the plastic deformation in the disc, resulting in the rubbing of metal-against-metal and thus adhesive wear. The improved wear resistance of the surface treated materials, to some degree, could also be attributed to the reduced metallurgical compatibility owing to the formation of the S-phase layer.

The type of corrosion–wear that was observed in this study was mechanically dominated with very mild corrosion. The mechanical component of the corrosion–wear of the untreated test pieces was attributed to adhesive, abrasive, oxidative and delamination wear. In the case of the treated specimens it was attributed mostly to abrasion and oxidation, with some cracking in nitrogen containing layers. According to the corrosion–wear mechanisms proposed by Dearnley et al. [18,19] the corrosion component was of Type I, which is the removal of the passive film during sliding contact and its subsequent regeneration. The other two types of mechanisms cannot be attributed because they are only related to coatings.

Cracking of the surface was noticed in most of the balls that were either nitrided or carbonitrided and all the discs which were nitrided. These cracks were always perpendicular to the direction of sliding (e.g. Fig. 16b). Because the nitrogen S-phase is very hard (Fig. 6) and could also be brittle; therefore when loaded it has a tendency to crack without strong support from the substrate. Although in Fig. 9 the wear resistance of nitrided surfaces appears to be good, these are not recommended for metal-on-metal joint application due to their tendency to crack. The hard S-phase containing wear debris would in turn cause aggravated wear especially if sliding against a softer material. Based on this work it can be concluded that a carbon S-phase engineered tribopair could be used as the bearing surfaces of joint prostheses.

5. Conclusions

1. All three plasma surface treatments, C500, N430 and NC430, can effectively improve the wear resistance of AISI 316 balls sliding in Ringer's solution against ASTM F138 and ASTM F1586 discs. This is mainly because of increased surface hardness and a strong support to the surface oxide film.
2. The combined wear of S-phase against S-phase for both ASTM F138 and ASTM F1586 materials is close to that of the cobalt-based tribopair under reciprocating sliding wear conditions in Ringer's solution at a maximum contact pressure of about 1.4 GPa.
3. S-phase surface engineering of austenitic stainless steels makes it possible for austenitic stainless steel to slide against austenitic stainless steel without causing scuffing or seizure. Therefore hardened austenitic stainless steels could compete against more expensive alloys, such as cobalt-based alloys, in wear applications such as that found in the food, pharmaceutical and biomedical industries.
4. The wear resistance of nitrided and carbonitrided surfaces appears to be good, however these are not recommended for metal-on-metal joint application due to their tendency to crack.

Acknowledgements

The authors would like to thank EPSRC (UK) for the financial support (EP/J018252/1 and EP/F006926/1) and ERDF (Malta) for the financing of the testing equipment through the project: "Developing an Interdisciplinary Material Testing and Rapid Prototyping R&D Facility (Ref. no. 012)". In addition, the authors wish to express their appreciation to their colleagues, Dr. X. Li, Dr. J. Chen and Mr. J. Camilleri for their technical support. Mr. D. Gouriou would like to thank Polytech Nantes, Université de Nantes, France for the financial support received to conduct an internship at the University of Malta. Dr. J. Buhagiar would like to thank the University of Malta and the University of Birmingham for their financial support.

References

[1] J.R. Davis, Stainless Steels, ASM International, Ohio, 1994.
[2] Z.L. Zhang, T. Bell, Structure and corrosion resistance of plasma nitrided stainless steel, Surface Engineering 1 (1985).
[3] D.B. Lewis, A. Leyland, P.R. Stevenson, J. Cawley, A. Matthews, Metallurgical study of low-temperature plasma carbon diffusion treatments for stainless steels, Surface and Coatings Technology 60 (1993) 416–423.
[4] C. Blawert, B.L. Mordike, G.A. Collins, K.T. Short, Y. Jiraskova, O. Schneeweiss, V. Perina, Characterisation of duplex layer structures produced by simultaneous implantation of nitrogen and carbon into austenitic stainless steel X5CrNi189, Surface and Coatings Technology 128–129 (2000) 219–225.
[5] S. Thaiwatthana, X.Y. Li, H. Dong, T. Bell, Corrosion wear behaviour of low temperature plasma alloyed 316 austenitic stainless steel, Surface Engineering 19 (2003) 211–216.
[6] G. Aldrich-Smith, D.G. Teer, P.A. Dearnley, Corrosion-wear response of sputtered CrN and S-Phase coated austenitic stainless steel, Surface and Coatings Technology 116–119 (1999) 1161–1165.
[7] A.J. Smith, P. Dieppe, K. Vernon, M. Porter, A.W. Blom, Failure rates of stemmed metal-on-metal hip replacements: analysis of data from the National Joint Registry of England and Wales, The Lancet 379 (2012) 1199–1204.
[8] H.C. Amstutz, M.J. Le Duff, Failure rates of stemmed metal-on-metal hip replacements, Lancet 380 (2012) 105.
[9] A.J. Smith, P. Dieppe, K. Vernon, M. Porter, A.W. Blom, Failure rates of stemmed metal-on-metal hip replacements—Authors' reply, The Lancet 380 (2012) 106.
[10] H. Dong, S-phase surface engineering of Fe–Cr, Co–Cr and Ni–Cr alloys, International Materials Review 55 (2010) 65–98.
[11] C.C.P.M. Verheyen, J.A.N. Verhaar, Failure rates of stemmed metal-on-metal hip replacements, The Lancet 380 (2012) 105.
[12] J. Chen, X.Y. Li, T. Bell, H. Dong, Improving the wear properties of Stellite 21 alloy by plasma surface alloying with carbon and nitrogen, Wear 264 (2008) 157–165.
[13] J. Buhagiar, T. Bell, R. Sammons, H. Dong, Evaluation of the biocompatibility of S-phase layers on medical grade austenitic stainless steels, Journal of Materials Science: Materials in Medicine 22 (2011) 1269–1278.
[14] X.Y. Li, J. Buhagiar, H. Dong, Characterisation of dual S phase layer on plasma carbonitrided biomedical austenitic stainless steels, Surf. Eng. 26 (2010) 72–78.
[15] J. Buhagiar, X. Li, H. Dong, Formation and microstructural characterisation of S-phase layers in Ni-free austenitic stainless steels by low-temperature plasma surface alloying, Surface and Coatings Technology 204 (2009) 330–335.
[16] K.C. Ludema, Friction, Wear, Lubrication: A Textbook in Tribology, CRC Press, Washington DC, 1996.
[17] I.M. Hutchings, Tribology: Friction and Wear of Engineering Materials, Edward Arnold, London, 1992.
[18] P.A. Dearnley, G. Aldrich-Smith, Corrosion–wear mechanisms of hard coated austenitic 316L stainless steels, Wear 256 (2004) 491–499.
[19] B. Mallia, P.A. Dearnley, The corrosion–wear response of Cr–Ti coatings, Wear 263 (2007) 679–690.